Deletion of the mu opioid receptor gene in mice reshapes the reward–aversion connectome

Anna E. Mechling[a,b], Tanzil Arefin[a,c], Hsu-Lei Lee[a], Thomas Bienert[a], Marco Reisert[a], Sami Ben Hamida[d,e], Emmanuel Darcq[e], Aliza Ehrlich[d,e], Claire Gaveriaux-Ruff[d], Maxime J. Parent[f], Pedro Rosa-Neto[f], Jürgen Hennig[a], Dominik von Elverfeldt[a], Brigitte Lina Kieffer[d,e,1,2], and Laura-Adela Harsan[a,g,h,1,2]

[a]Advanced Molecular Imaging Center, Medical Physics, University Medical Center Freiburg, 79106 Freiburg, Germany; [b]Faculty of Biology, University of Freiburg, 79104 Freiburg, Germany; [c]Bernstein Center for Computational Neuroscience, University of Freiburg, 79104 Freiburg, Germany; [d]Department of Translational Medicine and Neurogenetics, Institut de Génétique et de Biologie Moléculaire et Cellulaire, Illkirch-Graffenstaden 67400, France; [e]Department of Psychiatry, Douglas Hospital Research Center, School of Medicine, McGill University, Montreal, QC, Canada H3A 1A1; [f]Translational Neuroimaging Laboratory, Douglas Hospital Research Center, McGill University, Montreal, QC, Canada H3A 1A1; [g]Engineering Science, Computer Science, and Imaging Laboratory, Integrative Multimodal Imaging in Healthcare, UMR 7357, University of Strasbourg, CNRS, 67000 Strasbourg, France; and [h]Department of Biophysics and Nuclear Medicine, University Hospital Strasbourg, 67000 Strasbourg, France

Connectome genetics seeks to uncover how genetic factors shape brain functional connectivity; however, the causal impact of a single gene's activity on whole-brain networks remains unknown. We tested whether the sole targeted deletion of the mu opioid receptor gene (Oprm1) alters the brain connectome in living mice. Hypothesis-free analysis of combined resting-state fMRI diffusion tractography showed pronounced modifications of functional connectivity with only minor changes in structural pathways. Fine-grained resting-state fMRI mapping, graph theory, and intergroup comparison revealed Oprm1-specific hubs and captured a unique Oprm1 gene-to-network signature. Strongest perturbations occurred in connectional patterns of pain/aversion-related nodes, including the mu receptor-enriched habenula node. Our data demonstrate that the main receptor for morphine predominantly shapes the so-called reward/aversion circuitry, with major influence on negative affect centers.

mouse brain connectivity | resting-state functional MRI | diffusion tensor imaging | mu opioid receptor | reward/aversion network

Neuronal connectivity is at the foundation of brain function (1) and the concept that brain connectivity patterns are dynamically shaped by experience, pathology, and genetics has gained increasing importance. In humans, MRI has opened the era of connectome/imaging genetics to elucidate how genetic factors affect brain organization and connectivity in healthy individuals and disease, and to correlate genotype to phenotype (2). However, the causal impact of a single gene on overall functional connectivity (FC) remains largely unknown, and animal research is best suited to this goal. Here we tested whether combined functional/structural MRI in live animals (3–8) coupled to open-ended postprocessing analysis would reveal connectivity alterations upon targeted inactivation of a single gene. The mu opioid receptor (MOR) mediates the remarkably potent analgesic and addictive properties of opiates, like morphine (9), and belongs to the endogenous opioid system that controls sensory, emotional, and cognitive processes. This receptor is broadly distributed throughout the nervous system (10). It is a key component to facilitate reward (11) and relieves the negative experience of pain (12–14). In this report we show that targeted deletion of the MOR gene (Oprm1) significantly alters the brain connectome in living mice and predominantly reshapes the so-called reward/aversion network involved in pain, depression, and suicide (15).

Results and Discussion

Fine-Grained Mapping of the Mouse Brain Functional Connectome.

In a first step, we established fine-grained mapping of the mouse brain functional connectome (MBFC) in control and Oprm1$^{-/-}$ living mice. Using data-driven spatial independent component analysis (100-ICASSO) (4) of combined blood oxygenation level–dependent (BOLD) resting-state functional MRI (rsfMRI)

datasets (Materials and Methods, Data Analysis), we identified 87 functional components, the patterns of which covered neuroanatomical regions defined by automatic coregistration on the Allen Mouse Brain Atlas (AMBA; mouse.brain-map.org/static/atlas) (Fig. S1). We tested the reproducibility of the group ICASSO [a tool for reliability investigation of independent component analysis (ICA) estimates] patterns in each animal and in each experimental group separately via back-reconstruction (SI Materials and Methods, Statistical and Algorithmic Reliability of Group ICA Results and Fig. S2). These examples illustrate low intragroup variability of the ICA patterns and extremely high similarity between group patterns, supporting our further approach of using the 87 group ICA functional clusters (ICASSO components) as nodes in the generation of brain FC matrices of both Oprm1$^{-/-}$ and a control (Ctrl) group of animals (Materials and Methods, Data Analysis and SI Materials and Methods). These matrices, including both, correlations (positive) and anticorrelations (negative) between brain nodal activities (Fig. S3), were further used to examine whether global topological properties and organizational principles of the MBFC (4, 16) are modified in Oprm1$^{-/-}$ mice using graph theory (17). We probed small-world network hallmarks (SI Materials and Methods, Assessment of Global

---

Significance

Mice manipulated by targeted deletion of a specific brain gene show diverse pathological phenotypes, apparent, for example, in behavioral experiments. To explain observed findings, connectome genetics attempts to uncover how brain functional connectivity is affected by genetics. However the causal impact of a single gene on whole-brain networks is still unclear. Here the sole targeted deletion of the mu opioid receptor gene (Oprm1), the main target for morphine, induced widespread remodeling of brain functional connectome in mice. The strongest perturbations occurred within the so-called reward/aversion-circuitry, predominantly influencing the negative affect centers. We present a hypothesis-free analysis of combined structural and functional connectivity data obtained via MRI of the living mouse brain, and identify a specific Oprm1 gene-to-network signature.

NEUROSCIENCE

Topological Features of the MBFC in Ctrl and Oprm1^{-/-} Mice) and found similar features (Fig. S3) for both genotypes: a short average path length between all node pairs with high local clustering. We also tested modular properties (17) of the MBFC, a key feature of mammalian brain networks (18), and found partitioning into four stable functional modules (*SI Materials and Methods, Assessment of Global Topological Features of the MBFC in Ctrl and Oprm1^{-/-} Mice*) in both animal groups, indicating again that general organization principles of the MBFC are preserved in Oprm1^{-/-} mice.

However, this global analysis revealed that the recruitment of brain regions as network hubs (4, 19), defined as functional nodes showing above-mean normalized connectivity strength and diversity (*SI Materials and Methods, Assessment of Global Topological Features of the MBFC in Ctrl and Oprm1^{-/-} Mice*), was significantly modified in Oprm1^{-/-} mice. In the positive correlation analysis (Fig. S4), several components lost their hub status in Oprm1^{-/-} mice, suggesting decreased relay function in brain structures involved in positive affect and motivational processes [nucleus accumbens (ACB), prefrontal cortex (PFC)], as well as negative sensory and emotional experiences [midbrain reticular nucleus (MRN), periaqueductal gray (PAG), habenula (HB), somatosensory areas (SS)]. Concurrently, other nodes appeared as functional hubs in Oprm1^{-/-} mice only [caudoputamen (CP), bed nuclei of stria terminalis (BST), hippocampal formation (HPF) and peri-HPF cortex, thalamus (TH), superior colliculus (SC)/PAG, MRN/SC/PAG], which, without exception, covered areas integrated into the so-called core aversion-related network (20, 21). In addition, connectivity of PAG, which is a major opioid-sensitive pain-modulatory structure in both rodents (14,

22) and humans (23) and is engaged in aversive learning (24), appeared entirely remodeled in mutant mice (Fig. S4 B and C). Finally, the application of stronger exclusion criteria (combined positive and negative correlations) (Fig. S5) designated the ventro-medial rostral MRN/PAG as the sole remaining Oprm1-dependent functional hub. Together, these substantial hub alterations suggest facilitated communication across pain/aversion-processing centers and perhaps less-efficient integration of reward-related information.

Quantitative Intergroup Comparison of Ctrl and Oprm1^{-/-} Functional Connectomes Reveals an Oprm1^{-/-}-Specific Fingerprint. In a second step, we quantified remodeling of the Oprm1^{-/-} functional connectome using a direct statistical intergroup comparison of Ctrl and Oprm1^{-/-} MBFC matrices (*Materials and Methods, Direct Intergroup (Ctrl. vs. Oprm1^{-/-}) Statistical Analysis of MBFC* and Fig. 1). We detected significant and widespread alterations of internodes connectivity (Fig. 1) [$P < 0.05$, false-discovery rate (FDR) -corrected]. The 2D-matrix representation (Fig. 1A) captured the causal effect of targeted Oprm1 gene disruption at the level of whole-brain networks, and the extent of Oprm1-dependent connectional activity appeared surprisingly broad. To establish characteristic features of this Oprm1 FC signature, we ranked nodes on the basis of highest number of statistically significant differences in connectivity across the two genotypes (*Materials and Methods, Direct Intergroup (Ctrl. vs. Oprm1^{-/-}) Statistical Analysis of MBFC* and Fig. 1D). There was a clear dominance of connectivity changes for pain/aversion-related nodes [PAG, hippocampal region (HIP), amygdala (AMY), SS, anterior cingulate areas (ACA), MRN, HB], with the first top 10 of this hierarchy being core players of the
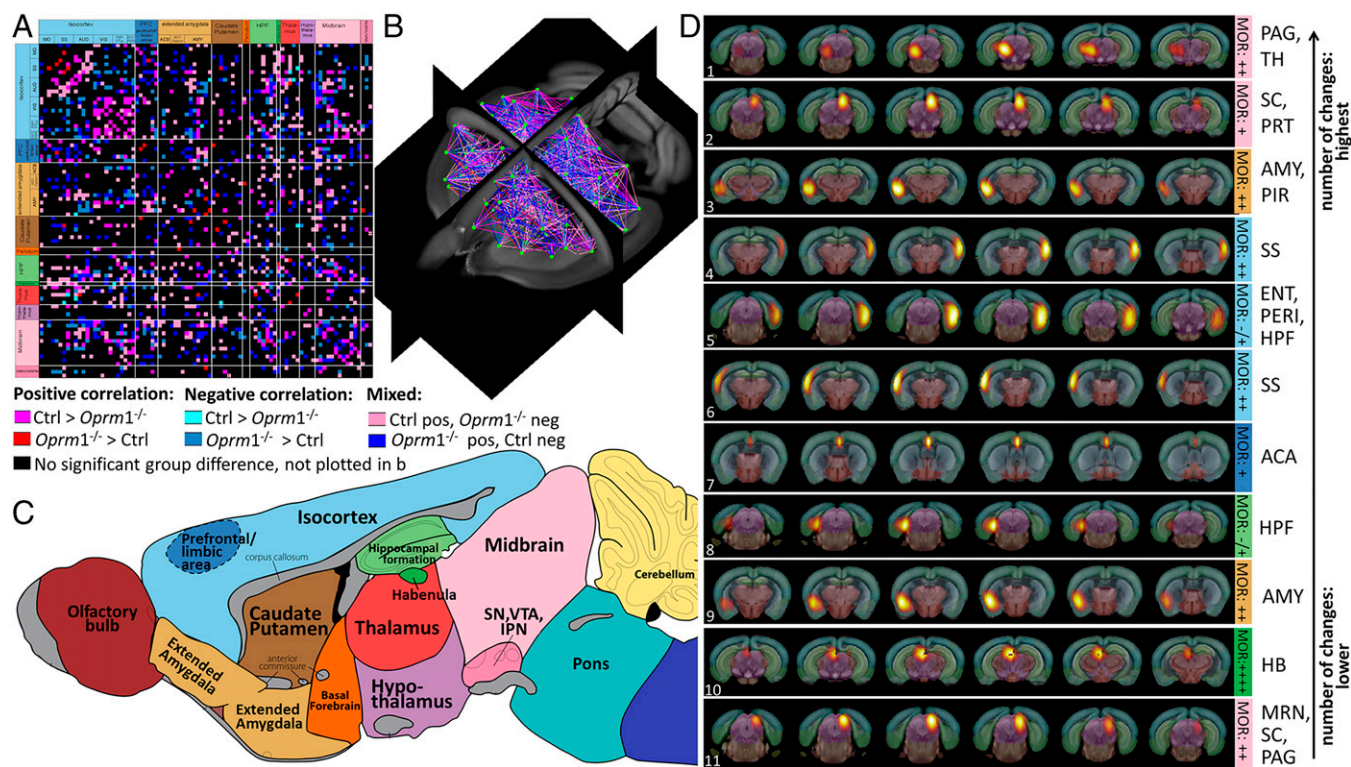
Fig. 1. Quantitative mapping of functional network alterations in Oprm1^{-/-} mice reveals a MOR-dependent activity signature in live animals. (A–C) Direct intergroup (Ctrl vs. Oprm1^{-/-}) statistical comparison of connectivity matrices ($P < 0.05$, FDR-corrected) is shown as a 2D-matrix (A) or a 3D view (B). Functional nodes were grouped and color-coded as assigned in the sagittal brain view from C. The Oprm1 genetic inactivation induced widespread modifications of internode connectivity. (D) Nodes with the highest number of statistically significant connectivity changes are ranked. Their functional pattern is overlaid on the Allen Brain Atlas, for precise anatomical identification. The top-10 nodes correspond to brain areas associated with pain/aversion processing or double players involved in both pain and reward (PAG/TH, SC/PRT, bilateral AMY, bilateral SS, and MRN/SC/PAG, ACA, HPF, HB). Information on MOR density (10) is included [from low "−/+" barely detectable in the entorhinal area (ENT)/perihinal area (PERI) cortex and HPF to "++++" highest expression in HB].

aversion-related network (20, 21). The intergroup comparative evaluation therefore leads to conclusions similar to the hub analysis (i.e., predominant reshaping of networks known to process information with negative valence).

Specifically, the ventro-lateral PAG (Fig. 1D, rank 1) showed the highest number of changes (Fig. 1D, Top, and Movie S1). In addition, the hippocampus, involved in early memory formation and responsive to pain in humans (25); the AMY, regulating

Fig. 2. MOR deletion predominantly reshapes the RAC, with a major impact on aversion-related components. (A) Detailed view into the matrix of significant connectivity alterations, corresponding to the three main nodes of RAC: PAG/TH (rank 1, see Fig 1D), HB (rank 10, see Fig 1D), and ACB (rank 37). Predominant alterations within reward/aversion pathways correlate with major behavioral modifications reported in mutant mice for pain, emotional, and reward-related behaviors (Dataset S1). (B–D) Three-dimensional display of significantly altered connections of functional nodes from A. The anatomical assignment corresponds to PAG/TH (B and Movie S1), pain/aversion component; HB (C and Movie S2), involved in both reward and aversion processing; and ACB (D and Movie S3), dominant role in reward processing. The three areas are also sites of high MOR density in the normal mouse brain. (E and F) Unified view of connectivity changes in the RAC circuitry of live Oprm1$^{-/-}$ brain. Key players of this circuitry are identified as follows: PFC, ACB, AMY, VTA/IPN, TH/PAG, HB, and SS (E). All modified connections are numbered and corresponding detailed connectivity patterns are provided in F. Functional pathways between two regions were considered altered when at least two functional nodes assigned to the respective anatomical areas change their direct connectional pattern.

affective dimensions of pain (26) (Fig. 1*D*; HPF ranks 5 and 8 and AMY ranks 3 and 9); and cortical connectivity, involved in aversion processing at high-order level (27) (Fig. 1*D*; SS ranks 4 and 6; ACA ranks 7) all showed strong FC perturbations. HB, covering the habenular complex that conveys negative reward-related information (28), was further ranked among nodes with highest connectivity changes (Fig. 1*D*, rank 10, and Movie S2). Of note, accumbens-related components were not among the top 10, although one ACB component showed above-threshold FC alterations (rank 37) (Movie S3). Coincident with the loss of hub function for the ACB/PFC node (Fig. S4), our data indicate detectable but only modest remodeling within this well-established brain substrate for reward processing (11, 29).

Genetic Inactivation of the MOR Reshapes the Reward/Aversion Runctional Circuitry. There is rising evidence that aversive and appetitive states interact to optimize adaptive behavioral choices and the existence of a reward/aversion circuitry (RAC) that would act as a unitary salience network has been proposed (30, 31). Because our statistical analysis reveals that the top-10 nodes all belong to the RAC (Fig. 1*D*), we isolated the *Oprm*1 signature for this particular network. Fig. 2 (see also Movies S1–S3) shows the major impact of *Oprm*1 gene activity on core components of the RAC in living mice and illustrates the notion that the *Oprm*1 fingerprint covers circuits encoding negative (PAG, HB, SS) rather than positive (ACB) dimensions of affective processing. We also extracted connectional patterns of the HB and ventral tegmental area/interpeduncular nucleus (VTA/IPN) nodes (Fig. 3 *A* and *B*), which represent key RAC circuitry components, expressing the highest density of MORs in the brain (Fig. 3 *C* and *D*). The FC organization was remarkably altered for these two nodes.

In particular, highly mixed rostro-caudal correlated/anticorrelated connections in control mice opposed prominent spatial segregation of correlated (mainly caudal) and anticorrelated (mainly rostral) connections in mutants (Fig. 3*A*). Thus, major changes of connectivity strength for the two nodes demonstrate concerted perturbation of the entire dorsal diencephalic conduction pathway (32) in *Oprm*1$^{-/-}$ mice.

Rich Remodeling of *Oprm*1$^{-/-}$ Functional Connectome Is Accompanied by Only Subtle Modifications of Structural Scaffolding Measured via Diffusion Tractography. Finally, we tested whether remodeling upon *Oprm*1 gene knockout was paralleled by modifications of the brain microstructure. We performed high-resolution fiber mapping of the structural connectivity (Movie S4) in the same animals (*Materials and Methods, Mouse Brain Tractography-Based Structural Network Analysis*). We used high angular-resolution diffusion imaging (HARDI) and global fiber tracking (3, 33). We found only subtle modifications of structural scaffolding (Fig. 4), contrasting the rich remodeling of FC and consistent with the neuromodulatory nature of the single missing gene (13, 34, 35).

Conclusions

In sum, unbiased analysis of MBFC in live *Oprm*1$^{-/-}$ mice reveals an *Oprm*1-specific FC signature, with strongest impact on the RAC connectome. Pain and pleasure are essential to shape learning and decision-making. The well-known dual analgesic/rewarding effects of morphine and the behavioral phenotypes of *Oprm*1$^{-/-}$ mutant mice showing increased pain perception (36) and reduced drug (37) or social (38, 39) reward, posit MOR as a central player for these fundamental processes. Indeed, two decades of *Oprm*1$^{-/-}$ mouse studies have unambiguously established

Fig. 3. Comparative 3D mapping of FC in *Oprm*1$^{-/-}$ and control mice for the MOR-enriched HB-VTA/IPN pathway. (*A*) FC mapping of HB and VTA/IPN nodes in control (*Left*, sagittal views) and *Oprm*1$^{-/-}$ brains (*Right*, sagittal views), extracted from the whole-brain FC matrices (Fig. S3) shows strong spatial segregation of anticorrelated (blue) and correlated (red) connections along the rostro-caudal brain axis in mutant animals. Highly mixed rostro-caudal correlated/anticorrelated connections are seen in control mice. The impact of the MOR deletion on internode connectivity strength is also represented (bar thickness). (*B*) The selected nodes are representative components of ICASSO analysis, anatomically assigned to HB and VTA/IPN (*Upper*). Statistical analysis (extracted from Fig. 1*A*) shows significant modification of FC between the two nodes, with negative correlation in the Ctrl and positive correlation in the *Oprm*1$^{-/-}$ group, respectively (see blue line). (*C* and *D*) MOR expression in HB and VTA/IPN, and along the fasciculus retroflexus (fr), with subcellular resolution (32). These brain areas are particularly rich in MOR expression, as shown in coronal (*C*) and sagittal (*D*) sections from MOR-mCherry knockin mice, with images acquired on slide scanner. (Magnification: *Inset*, 20×.) Reprinted with permission from ref. 32. In these mice the MOR protein, fused to a red-fluorescent protein, is directly visible in mouse tissues. Arrows point to MOR at the level of medial HB and IPN. Views correspond to both sagittal (*A*) and coronal (*B*) representations from the rsfMRI.
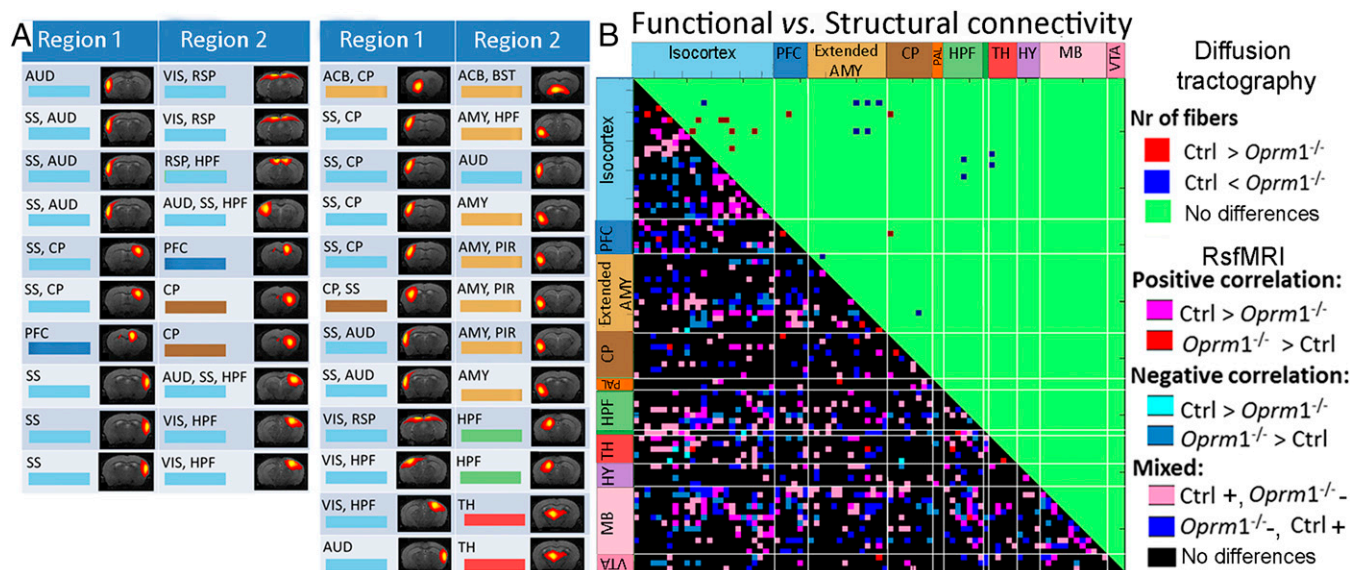
Fig. 4. Limited alteration of tractography-based structural compared with FC in *Oprm*1$^{-/-}$ mice. (*A*) Modifications of internode structural connectivity: changes were assessed based on the number of fibers directly connecting functional nodes of the brain connectivity matrix (between region 1 and region 2). (*Left*) Significant change in fiber numbers Ctrl > *Oprm*1$^{-/-}$. (*Right*) Significant change in fiber numbers *Oprm*1$^{-/-}$ > Ctrl. (*B*) Direct comparison of significant functional and structural connectivity showed widespread FC modifications in mutant mice, whereas structural adaptations were limited. The few alterations of structural connectivity determined from tractography included SS, AMY, and ACB, as well as SS–AMY connections. Diffusion tractography also showed remodeling within ACB (*A*, first row right) in MOR depleted brains but no modification for midbrain centers (i.e., PAG).

the pivotal role of MOR in both pain and pleasure (Dataset S1 and references therein), recognized as intermingled processes at circuit level (40) and for pathology (41).

In our analysis, the major influence of *Oprm*1 inactivation on aversion/pain-related, rather than reward connectivity, may reflect a stronger inhibitory MOR tone or developmental influence on negative affect centers, at least under resting-state conditions. From an evolutionary perspective, pain represents a key signal for survival, and successful coping with a pain stimulus is essential to gain a selective advantage (42). Despite the antique notion that pain and pleasure form a continuum, it is only recently that the rewarding value of pain relief has been recognized (40, 41). The key implication of MOR activity in dampening physical, emotional, and social pain, evidenced in human PET imaging studies (see ref. 43 and references therein), and our own FC analysis of live *Oprm*1-deficient mice, together suggest that pain relief may be a primary MOR function.

Importantly, our data unequivocally reveal pronounced causal effects of a single gene on whole-brain FC in live animals, with subtle modifications of the tractography-based structural connectome. This report is among the very first studies (44) that open the way to targeted connectome genetics (2) in basic research and, to the best of our knowledge, this is the first hypothesis-free analysis of combined rsfMRI/diffusion tractography data in the mouse, leading to the identification of a specific gene-to-network signature.

Materials and Methods

Ethics. All experiments were performed in accordance with the German and French laws and guidelines regarding ethics on animal experimentation (ethics allowance 35_9185.81/G-13/15).

Animal Preparation, Anesthesia, and Physiological Parameters. Animal preparation, anesthesia, and physiological parameters during imaging are described in the first part of *SI Materials and Methods*. The rsfMRI data were acquired under continuous Medetomidine (MD, an α-2 adrenergic agonist) sedation through a MRI compatible catheter (initial intraperitoneal injection of 0.3 mg MD per kilogram body weight in 100 μL 0.9% NaCl-solution followed by subcutaneous infusion of 0.6 mg per kilogram body weight in 200 μL/h). MD was selected among other anesthetics based on previous reports suggesting minimal impact on FC (5, 45–47).

Mouse Brain MRI Data Acquisition. Mouse brain MRI data acquisition (see also *SI Materials and Methods*) was performed with a 7T animal scanner (Biospec 70/20) and a mouse head-adapted cryocoil (both from Bruker). rsfMRI data were collected (30 min after MD bolus injection) using single-shot Gradient Echo Echo Planar Imaging (EPI) [12 axial slices, 200 volumes, image resolution $150 \times 150 \times 700$ μm^3, echo time (TE)/repetition time (TR) = 10 ms/1,700 ms]. High-resolution morphological imaging was done using Turbo RARE T$_2$ (51 × 51×300 μm^3, TE/TR = 50 ms/6,514 ms). HARDI was performed using a four-shot Diffusion Tensor Imaging–EPI (DTI–EPI) sequence (15 axial slices, resolution of $94 \times 94 \times 500$ μm^3, TE/TR = 27 ms/3,750 ms); Δ = 10 ms, diffusion gradient duration (δ) = 5 ms, b$_{factor}$ = 1,000 s/mm^2, 30 diffusion gradient directions.

Data Analysis. The data preprocessing pipeline is described in *SI Materials and Methods*.

rsfMRI data analysis. Identification of elementary functional clusters as nodes of the MBFC matrix was performed via high-dimensional ICA (100 components). Spatial group ICA (48) via the MATLAB based toolbox GIFT (Group ICA of fMRI Toolbox, v1.3i, www.nitrc.org/projects/gift/) was carried out on all of the mouse brain rsfMRI data (*Oprm*1$^{-/-}$ and Ctrl mice) using the Infomax algorithm. ICASSO (49) was used to assess pattern stability for the identified components (*SI Materials and Methods*, *Statistical and Algorithmic Reliability of Group ICA Results*). The mean resulting patterns were displayed as spatial color-coded z-maps onto T$_2$ weighted images and on coregistered AMBA (50) (see, for example, Figs. 1–3, Figs. S1, S4, and S5, and Movies S1–S3). Coregistration with AMBA allowed for automatic identification of anatomic brain areas covered by IC patterns. From the 100-ICASSO results, 13 artifactual components were excluded from analysis. The meaningful 87 functional clusters were further used as nodes (Fig. S1) in the generation of the MBFC matrix, via partial correlation (PC).

PC analysis (*SI Materials and Methods*, *Partial Pearson Correlation*) was performed for each experimental group (*Oprm*1$^{-/-}$ and Ctrl) separately. The time courses associated with each relevant independent component (IC, node) obtained from 100-ICASSO were used in PC analysis using an in-house developed MATLAB tool (4). The PC coefficients (Pearson) between each pair of IC were calculated and used to create a 87 × 87 adjacency PC matrix for each animal, as well as two average matrices, representative for each experimental group (*Oprm*1$^{-/-}$ and Ctrl) (Fig. S3E; see also and histogram display of correlation coefficients in Fig. S3F). Each element of the matrix represented the strength of direct connectivity between two components (nodes). The PC matrices were then normalized using Fisher's z transformation. The significance of positive and negative correlations between pairs of components was further assessed via a two-sided one-sample *t* test, for *P* < 0.05 (4). This procedure generated a weighted undirected matrix

NEUROSCIENCE

(WUM) for each group, containing statistically relevant/significant correlation values. For 3D visualization of the MBFC, a Matlab-based toolbox was developed (*SI Materials and Methods*, *Visualization of Results*).

Assessment of global topological features of the MBFC in Ctrl and *Oprm*1$^{-/-}$ mice is described in *SI Materials and Methods*.

Direct intergroup (Ctrl vs. 0prm1$^{-/-}$) statistical analysis of MBFC. The analysis of the FC remodeling of the *Oprm*1$^{-/-}$ mouse brain was done via direct statistical comparison between the PC matrices (unthresholded *z* matrices) generated for each experimental group. We tested the hypothesis that there are no differences in connectivity between the two groups via a two-sided two-sample *t* test (similar variation within each group). The hypothesis was rejected at a significance level of 0.05, under FDR control for multiple comparisons.

A group comparison matrix (GCM) was generated (Fig. 2*A*) that color-coded the statistically significant intergroup differences of connectivity. Each node was associated to a broader brain area, based on the anatomical overlapping assigned via coregistration of the ICA results on the AMBA. The GCM was arranged to cluster the connectivity changes in association to anatomical areas (Fig. 1 *A* and *C* and Fig. S1). Three-dimensional visualization of

the changed connections was also generated (Fig. 1*B*). The color-code associated with the GCM was maintained for the 3D displays. Only nodes showing changes in their FC are plotted. The GCM was further used to count the significantly changed connections for each node (IC) and we further ranked nodes on the basis of highest number of such statistically significant differences in connectivity across the two genotypes (Fig. 1*D*).

Mouse brain tractography-based structural network analysis. Mouse brain tractography-based structural network analysis are detailed in *SI Materials and Methods*, *Mouse Brain Structural Network Analysis*.

1. Van Essen DC (2013) Cartography and connectomes. *Neuron* 80(3):775–790.
2. Thompson PM, Ge T, Glahn DC, Jahanshad N, Nichols TE (2013) Genetics of the connectome. *Neuroimage* 80:475–488.
3. Harsan LA, et al. (2013) Mapping remodeling of thalamocortical projections in the living reeler mouse brain by diffusion tractography. *Proc Natl Acad Sci USA* 110(19):E1797–E1806.
4. Mechling AE, et al. (2014) Fine-grained mapping of mouse brain functional connectivity with resting-state fMRI. *Neuroimage* 96:203–215.
5. Grandjean J, Schroeter A, Batata I, Rudin M (2014) Optimization of anesthesia protocol for resting-state fMRI in mice based on differential effects of anesthetics on functional connectivity patterns. *Neuroimage* 102(Pt 2):838–847.
6. Gozzi A, Schwarz AJ (2016) Large-scale functional connectivity networks in the rodent brain. *Neuroimage* 127:496–509.
7. Stafford JM, et al. (2014) Large-scale topology and the default mode network in the mouse connectome. *Proc Natl Acad Sci USA* 111(52):18745–18750.
8. Zerbi V, et al. (2014) Resting-state functional connectivity changes in aging apoE4 and apoE-KO mice. *J Neurosci* 34(42):13963–13975.
9. Matthes HW, et al. (1996) Loss of morphine-induced analgesia, reward effect and withdrawal symptoms in mice lacking the mu-opioid-receptor gene. *Nature* 383(6603):819–823.
10. Erbs E, et al. (2015) A mu-delta opioid receptor brain atlas reveals neuronal co-occurrence in subcortical networks. *Brain Struct Funct* 220(2):677–702.
11. Le Merrer J, Becker JA, Befort K, Kieffer BL (2009) Reward processing by the opioid system in the brain. *Physiol Rev* 89(4):1379–1412.
12. Leknes S, Tracey I (2008) A common neurobiology for pain and pleasure. *Nat Rev Neurosci* 9(4):314–320.
13. Navratilova E, Porreca F (2014) Reward and motivation in pain and pain relief. *Nat Neurosci* 17(10):1304–1312.
14. Fields H (2004) State-dependent opioid control of pain. *Nat Rev Neurosci* 5(7):565–575.
15. Elman I, Borsook D, Volkow ND (2013) Pain and suicidality: Insights from reward and addiction neuroscience. *Prog Neurobiol* 109:1–27.
16. Liang Z, Li T, King J, Zhang N (2013) Mapping thalamocortical networks in rat brain using resting-state functional connectivity. *Neuroimage* 83:237–244.
17. Bullmore E, Sporns O (2009) Complex brain networks: Graph theoretical analysis of structural and functional systems. *Nat Rev Neurosci* 10(3):186–198.
18. Fornito A, Zalesky A, Breakspear M (2015) The connectomics of brain disorders. *Nat Rev Neurosci* 16(3):159–172.
19. Liska A, Galbusera A, Schwarz AJ, Gozzi A (2015) Functional connectivity hubs of the mouse brain. *Neuroimage* 115:281–291.
20. Hayes DJ, Northoff G (2011) Identifying a network of brain regions involved in aversion-related processing: A cross-species translational investigation. *Front Integr Nuerosci* 5:49.
21. Hayes DJ, Northoff G (2012) Common brain activations for painful and non-painful aversive stimuli. *BMC Neurosci* 13:60.
22. Linnman C, Moulton EA, Barmettler G, Becerra L, Borsook D (2012) Neuroimaging of the periaqueductal gray: State of the field. *Neuroimage* 60(1):505–522.
23. Wager TD, Scott DJ, Zubieta JK (2007) Placebo effects on human mu-opioid activity during pain. *Proc Natl Acad Sci USA* 104(26):11056–11061.
24. Roy M, et al. (2014) Representation of aversive prediction errors in the human periaqueductal gray. *Nat Neurosci* 17(11):1607–1612.
25. Forkmann K, et al. (2013) Pain-specific modulation of hippocampal activity and functional connectivity during visual encoding. *J Neurosci* 33(6):2571–2581.
26. Neugebauer V (2015) Amygdala pain mechanisms. *Handbook Exp Pharmacol* 227:261–284.
27. Bushnell MC, Ceko M, Low LA (2013) Cognitive and emotional control of pain and its disruption in chronic pain. *Nat Rev Neurosci* 14(7):502–511.
28. Hikosaka O (2010) The habenula: from stress evasion to value-based decision-making. *Nat Rev Neurosci* 11(7):503–513.
29. Russo SJ, Nestler EJ (2013) The brain reward circuitry in mood disorders. *Nat Rev Neurosci* 14(9):609–625.
30. Borsook D, et al. (2007) Reward-aversion circuitry in analgesia and pain: Implications for psychiatric disorders. *Eur J Pain* 11(1):7–20.
31. Lammel S, et al. (2012) Input-specific control of reward and aversion in the ventral tegmental area. *Nature* 491(7423):212–217.
32. Gardon O, et al. (2014) Expression of mu opioid receptor in dorsal diencephalic conduction system: New insights for the medial habenula. *Neuroscience* 277:595–609.
33. Reisert M, et al. (2011) Global fiber reconstruction becomes practical. *Neuroimage* 54(2):955–962.
34. Loseth GE, Ellingsen DM, Leknes S (2014) State-dependent μ-opioid modulation of social motivation. *Front Behav Neurosci* 8:430.
35. Navratilova E, et al. (2015) Endogenous opioid activity in the anterior cingulate cortex is required for relief of pain. *J Neurosci* 35(18):7264–7271.
36. Kieffer BL, Gavériaux-Ruff C (2002) Exploring the opioid system by gene knockout. *Prog Neurobiol* 66(5):285–306.
37. Contet C, Kieffer BL, Befort K (2004) Mu opioid receptor: A gateway to drug addiction. *Curr Opin Neurobiol* 14(3):370–378.
38. Moles A, Kieffer BL, D'Amato FR (2004) Deficit in attachment behavior in mice lacking the mu-opioid receptor gene. *Science* 304(5679):1983–1986.
39. Becker JA, et al. (2014) Autistic-like syndrome in mu opioid receptor null mice is relieved by facilitated mGluR4 activity. *Neuropsychopharmacology* 39(9):2049–2060.
40. Navratilova E, Atcherley CW, Porreca F (2015) Brain circuits encoding reward from pain relief. *Trends Neurosci* 38(11):741–750.
41. Elman I, Borsook D (2016) Common brain mechanisms of chronic pain and addiction. *Neuron* 89(1):11–36.
42. Fields HL (2014) Neuroscience. More pain; less gain. *Science* 345(6196):513–514.
43. Hsu DT (2015) It still hurts: Altered endogenous opioid activity in the brain during social rejection and acceptance in major depressive disorder. *Mol Psychiatry* 20(2):193–200.
44. Zhan Y, et al. (2014) Deficient neuron-microglia signaling results in impaired functional brain connectivity and social behavior. *Nat Neurosci* 17(3):400–406.
45. Weber R, Ramos-Cabrer P, Wiedermann D, van Camp N, Hoehn M (2006) A fully noninvasive and robust experimental protocol for longitudinal fMRI studies in the rat. *Neuroimage* 29(4):1303–1310.
46. Pawela CP, et al. (2009) A protocol for use of medetomidine anesthesia in rats for extended studies using task-induced BOLD contrast and resting-state functional connectivity. *Neuroimage* 46(4):1137–1147.
47. Nasrallah FA, Tay HC, Chuang KH (2014) Detection of functional connectivity in the resting mouse brain. *Neuroimage* 86:417–424.
48. Calhoun VD, Adali T, Pearlson GD, Pekar JJ (2001) A method for making group inferences from functional MRI data using independent component analysis. *Hum Brain Mapp* 14(3):140–151.
49. Himberg J, Hyvärinen A, Esposito F (2004) Validating the independent components of neuroimaging time series via clustering and visualization. *Neuroimage* 22(3):1214–1222.
50. Lein ES, et al. (2007) Genome-wide atlas of gene expression in the adult mouse brain. *Nature* 445(7124):168–176.
51. van de Ven VG, Formisano E, Prvulovic D, Roeder CH, Linden DE (2004) Functional connectivity as revealed by spatial independent component analysis of fMRI measurements during rest. *Hum Brain Mapp* 22(3):165–178.
52. Margulies DS, et al. (2010) Resting developments: A review of fMRI post-processing methodologies for spontaneous brain activity. *MAGMA* 23(5–6):289–307.
53. Esposito F, et al. (2003) Real-time independent component analysis of fMRI time-series. *Neuroimage* 20(4):2209–2224.
54. Moritz CH, Carew JD, McMillan AB, Meyerand ME (2005) Independent component analysis applied to self-paced functional MR imaging paradigms. *Neuroimage* 25(1):181–192.
55. Li YO, Adali T, Calhoun VD (2007) Estimating the number of independent components for functional magnetic resonance imaging data. *Hum Brain Mapp* 28(11):1251–1266.
56. Smith SM, et al. (2011) Network modelling methods for FMRI. *Neuroimage* 54(2):875–891.
57. Watts DJ, Strogatz SH (1998) Collective dynamics of 'small-world' networks. *Nature* 393(6684):440–442.
58. Humphries MD, Gurney K, Prescott TJ (2006) The brainstem reticular formation is a small-world, not scale-free, network. *Proc Biol Sci* 273(1585):503–511.
59. Newman ME (2006) Modularity and community structure in networks. *Proc Natl Acad Sci USA* 103(23):8577–8582.
60. Rubinov M, Sporns O (2010) Complex network measures of brain connectivity: Uses and interpretations. *Neuroimage* 52(3):1059–1069.